THE JOURNAL OF BIOLOGICAL CHEMISTRY VOL. 286, NO. 40, pp. 34627–34634, October 7, 2011

Engineering the Respiratory Complex I to Energy-converting NADPH:Ubiquinone Oxidoreductase*[S]

Received for publication, June 22, 2011, and in revised form, August 9, 2011 Published, JBC Papers in Press, August 10, 2011, DOI 10.1074/jbc.M111.274571

Klaudia Morina, Marius Schulte, Florian Hubrich, Katerina Dörner, Stefan Steimle, Stefan Stolpe, and Thorsten Friedrich[1]

From the Institut für Organische Chemie und Biochemie, Albert-Ludwigs-Universität, 79104 Freiburg, Germany

Background: Respiratory complex I accepts electrons from NADH.
Results: Mutation of a single amino acid residue leads to a physiological oxidation of NADPH, however, coupled with the production of reactive oxygen species.
Conclusion: The NADH-binding site of complex I evolved to discriminate NADH from NADPH and to reduce the production of reactive oxygen species.
Significance: The mode of nucleotide binding determines the production of reactive oxygen species in complex I.

The respiratory complex I couples the electron transfer from NADH to ubiquinone with a translocation of protons across the membrane. Its nucleotide-binding site is made up of a unique Rossmann fold to accommodate the binding of the substrate NADH and of the primary electron acceptor flavin mononucleotide. Binding of NADH includes interactions of the hydroxyl groups of the adenosine ribose with a conserved glutamic acid residue. Structural analysis revealed that due to steric hindrance and electrostatic repulsion, this residue most likely prevents the binding of NADPH, which is a poor substrate of the complex. We produced several variants with mutations at this position exhibiting up to 200-fold enhanced catalytic efficiency with NADPH. The reaction of the variants with NAD(P)H is coupled with proton translocation in an inhibitor-sensitive manner. Thus, we have created an energy-converting NADPH:ubiquinone oxidoreductase, an activity so far not found in nature. Remarkably, the oxidation of NAD(P)H by the variants leads to an enhanced production of reactive oxygen species.

The NADH:ubiquinone oxidoreductase, also known as respiratory complex I,[2] couples the transfer of electrons from NADH to ubiquinone with the translocation of protons across the membrane (1–6). In doing so, it contributes to the generation of the protonmotive force required for energy-consuming processes. In eukaryotes, complex I consists of 45 different subunits resulting in a molecular mass of about 1 MDa (7). The bacterial homologue generally consists of 14 subunits named NuoA to NuoN (or Nqo1–14). Both the mitochondrial and the bacterial complex contain the same cofactors for the electron transfer reaction, namely one flavin mononucleotide (FMN) and up to 10 iron-sulfur (Fe/S) clusters (8). Because of this, the bacterial complex I is regarded as a simple structural and functional model for the eukaryotic enzyme (9). Electron microscopy revealed the two-part structure of the complex consisting of a peripheral and a membrane arm (10, 11). In bacteria, the peripheral arm is made up of seven globular subunits, and the membrane arm consists of seven polytopic subunits comprising 63 transmembrane helices. All known cofactors and the NADH-binding site are located within the peripheral arm, the structure of which was resolved at 3.3 Å resolution (12, 13). The quinone reduction site is proposed to be located at the interface between the peripheral and the membrane arm (14, 15). The membrane arm lacks any known cofactor but has to be involved in proton translocation. This is supported by the homology of the three major subunits of the arm to subunits of cation/proton antiporters (16, 17). Mechanisms based on a conformational link between the redox reaction and the proton translocation have been discussed (4, 5, 18, 19). The recently published crystal structures of complex I from *Thermus thermophilus* (20) and *Yarrowia lipolytica* (21) imply that the complex contains a coupling site directly linked to electron transfer as well as another site indirectly coupled with electron transfer.

NADPH is known to be a very poor substrate for the complex (22). It was established that submitochondrial particles exhibit an NADPH oxidase activity (23). The optimum for this activity is around pH 6, whereas the NADH oxidase activity shows a broad optimum around pH 7. The NADPH oxidase activity was about one-fifth of the NADH oxidase activity at pH 6 (24). The activity was shown to be an intrinsic property of the mitochondrial complex I and not related to the activity of the NADPH/NAD transhydrogenase (23, 24). The structure of the peripheral arm of complex I with NADH bound to subunit NuoF revealed that the carboxylate group of Glu-183^F (nomenclature according to the *Escherichia coli* sequence; the superscript denotes the name of the corresponding Nuo subunit) is hydrogen-bonded to the hydroxyl groups of the adenosine ribose

* This work was supported by the Volkswagen Stiftung and the Deutsche Forschungsgemeinschaft.
[S] The on-line version of this article (available at http://www.jbc.org) contains supplemental Tables S1–S6 and Figs. S1–S3.
[1] To whom correspondence should be addressed: Albert-Ludwigs-Universität, Institut für Organische Chemie und Biochemie, Albertstr. 21, Chemiehochhaus, 79104 Freiburg, Germany. Fax: 49-761-203-6096; E-mail: tfriedri@uni-freiburg.de.
[2] The abbreviations used are: complex I, proton-pumping NADH:ubiquinone oxidoreductase; ACMA, 9-amino-6-chloro-2-methoxyacridine; CCCP, carbonyl cyanide *m*-chlorophenylhydrazone; Fe/S, iron-sulfur; decyl-ubiquinone, 2,3-dimethoxy-5-methyl-6-decylbenzoquinone; ROS, reactive oxygen species; mT, millitesla; DEPMPO, 5-(diethoxyphosphoryl)-5-methyl-1-pyrroline-*N*-oxide, (2-methyl-3,4-dihydro-1-oxide-2*H*-pyrrol-2-yl)diethylphosphonate.

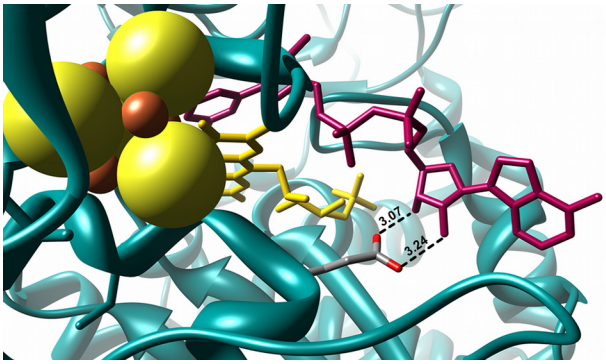

FIGURE 1. **Structure of the nucleotide-binding site of complex I with bound NADH.** The protein is shown in *blue*, iron in *red*, sulfur in *yellow*, the FMN in *yellow*, and the bound NADH in *magenta*. The radius of the sulfur ion was set to 1.7 Å and that of the iron ions to 0.7 Å (48). The length of the hydrogen bonds between Glu-183^F and the adenosine ribose hydroxyl groups are given in Å. The picture was drawn with Chimera (49) using the Protein Data Bank code 3IAM (13).

(13). The ribose is shielded by the protein in such a way that there is some but not sufficient space below the O^{2B} atom to provide space for the phosphate group of NADPH (Fig. 1), thus explaining its low reactivity with complex I. In principle, NADPH could be a substrate for the complex, but most likely due to the steric hindrance and electrostatic repulsion with Glu-183^F, its reaction rate with NADPH is at least five times slower than with NADH as a substrate (24, 25). Here, we report on engineering complex I to an energy-converting NADPH: ubiquinone oxidoreductase by a single mutation of the conserved Glu-183^F.

EXPERIMENTAL PROCEDURES

Materials and Strains—A derivative from *E. coli* strain BW25113 (26) was used, in which the *nuo*-operon was deleted by genomic replacement methods (27).[3] In addition, *E. coli* strain DH5α*Δnuo* (28) and the plasmids pBAD*nuo*$_{His}$ (29), pCA24N*nuoF* (30), and pKD46 (28) were used. Chloramphenicol (170 μg/ml), ampicillin (100 μg/ml), and kanamycin (50 μg/ml) were supplemented where necessary. All enzymes used for recombinant DNA techniques were from Fermentas (St. Leon-Roth, Germany). DNA oligonucleotides were from MWG Operon (Ebersberg, Germany).

Site-directed Mutagenesis—The plasmid pCA24N*nuoF* (30) was used to introduce mutations in *nuoF*. The primer pairs *nuoF* E183D, *nuoF* E183H, *nuoF* E183N, and *nuoF* E183Q (supplemental Table S1) were used to create the plasmids pCA24N*nuoF* E183D/E183H/E183N and E183Q.

λ-Red-mediated Recombineering—Electrocompetent DH5-α*Δnuo*/pKD46 cells were prepared and electroporated (28). The *nptI-sacRB* cartridge was amplified from pVO1100 by PCR with the primer pair *nuoF*::*nptI-sacRB* (supplemental Table S2). To integrate the cartridge into pBAD*nuo*$_{His}$ by λ-Red-mediated recombineering (27), electrocompetent DH5α*Δnuo*/pKD46 was mixed with 50 ng of pBAD*nuo*$_{His}$ and 350 ng of the PCR product. Recombinants were selected on LB-agar supplemented with kanamycin. Plasmids were isolated from Km^R clones and purified by transformation of DH5α and growth on LB-agar supplemented with kanamycin. The *nptI-sacRB* cartridge on pBAD*nuo*$_{His}$ was replaced by the PCR product containing the mutation by recombineering. A linear dsDNA was amplified from pCA24N*nuoF* carrying the point mutation by PCR with the primer pair *nuoF*2_fwd and *nuoF*_rev (supplemental Table S2). Electrocompetent DH5α*Δnuo*/pKD46 was co-transformed with 50 ng pBAD*nuo*$_{His}$ *nuoF*::*nptI-sacRB* and 400–500 ng of PCR product. Recombinants were selected on YP-agar supplemented with chloramphenicol and 10% (w/v) sucrose at 30 °C. Plasmids from Cam^R and Suc^R clones were isolated. All mutations were confirmed by DNA sequencing.

Isolation of Complex I and the Variants—The complex and its variants were isolated as described (29). Typical course of the preparations is shown in supplemental Tables S3–S6.

Determination of Complex I Activity—*E. coli* cytoplasmic membranes were isolated as described (31). The NAD(P)H oxidase activity of the cytoplasmic membranes was measured with a Clark-type oxygen electrode at 30 °C. The assay contained ~200 μg of membrane protein in 50 mM MES/NaOH, 50 mM NaCl, 5 mM $MgCl_2$, pH 6.0. The reaction was started by adding 2.5 mM of either NADH or NADPH (both from Sigma), respectively. After 1 min, 10 μM piericidin A was added to the assay. The NAD(P)H:decyl-ubiquinone oxidoreductase activity of the isolated complex was measured either as a decrease of the NAD(P)H concentration at 340–400 nm using an ε of 6.3 mM^{-1} cm^{-1} or as a decrease in the decyl-ubiquinone concentration at 248–268 nm using an ε of 7.8 mM^{-1} cm^{-1} (32). The very high NADPH concentrations were measured at 378–400 nm using an ε of 1.59 mM^{-1} cm^{-1}. The enzyme was reconstituted in *E. coli* polar lipids (Avanti) by mixing the preparation (10 mg/ml) in 1:1 (w/w) ratio with the lipids (10 mg/ml) and by incubating for 20 min on ice. One μl of the protein/lipid mixture (or 3 μl with NADPH as substrate for the complex from the parental strain) was added to the assay buffer (50 mM MES/NaOH, 50 mM NaCl, pH 6.0) at 30 °C. The assay for the determination of the K_M to NAD(P)H contained 60 μM decyl-ubiquinone, and the reaction was started by an addition of the corresponding nucleotide in various concentrations. The pH dependence of the NAD(P)H:decyl-ubiquinone oxidoreductase activity was assayed in the range from pH 5.0 to 8.0 using 50 mM MES, MOPS, or Tris as buffers. At lower pH values, the Fe/S clusters fall apart, and at higher values, the *E. coli* complex I disintegrates (8).

Determination of a Proton Gradient—The generation of a proton gradient was determined by the fluorescence quench of 9-amino-6-chloro-2-methoxyacridine (ACMA, Sigma). Proteoliposomes containing complex I were prepared as described (32). Five μl of proteoliposomes, 0.2 μM ACMA, and 50 μM decyl-ubiquinone were incubated for 3 min at 25 °C in 5 mM MES/NaOH, 50 mM KCl, 2 mM $MgCl_2$, pH 6.0. The fluorescence was detected with an LS 45 luminescence spectrometer (PerkinElmer Life Sciences), using an excitation wavelength of 430 nm and an emission wavelength of 480 nm. The reaction was started by an addition of 150 μM nucleotide. In control experiments either 20 μM CCCP or 20 μM piericidin A was added to the reaction mixture.

EPR Spectroscopy—EPR measurements were conducted with a Bruker EMX 1/6 spectrometer operating at X-band (9.2 GHz).

[3] M. Vranas and T. Friedrich, unpublished results.

TABLE 1

Kinetic parameters of the NAD(P)H:decyl-ubiquinone oxidoreductase activity of *E. coli* complex I and variants of the complex after reconstitution in phospholipids

Activity was determined by measuring the rate of NAD(P)H oxidation.

Variant	K_M		V_{max}		k_{cat}		k_{cat}/K_M	
	NADH	NADPH	NADH	NADPH	NADH	NADPH	NADH	NADPH
	μM		μmol·min^{-1}·mg^{-1}		s^{-1}		$s^{-1}\cdot\mu M^{-1}$	
Parental	13.0 ± 1	1,870 ± 30	2.9 ± 0.2	0.4 ± 0.1	26 ± 2	3 ± 1	2.0 ± 0.3	0.0018 ± 0.001
E183D^F	5.8 ± 1	390 ± 30	4.2 ± 0.2	3.8 ± 0.2	37 ± 2	34 ± 2	6.4 ± 0.4	0.09 ± 0.006
E183Q^F	12.0 ± 2	45 ± 4	3.1 ± 0.2	1.6 ± 0.1	28 ± 2	14 ± 1	2.3 ± 0.5	0.32 ± 0.003
E183N^F	14.0 ± 1	480 ± 50	1.2 ± 0.2	1.2 ± 0.3	11 ± 2	11 ± 3	0.8 ± 0.1	0.02 ± 0.006
E183H^F	5.7 ± 1	25 ± 2	4.1 ± 0.2	1.1 ± 0.1	37 ± 2	10 ± 1	6.5 ± 0.3	0.40 ± 0.003

The sample temperature was controlled with an Oxford instrument ESR-9 helium flow cryostat. The magnetic field was calibrated using a strong pitch standard. The isolated proteins (5 mg/ml) were reduced with a 1,000-fold molar excess NAD(P)H and frozen after a 30 s incubation on ice. The reaction tubes and the EPR tubes were flushed with nitrogen before filling to prevent oxidation by air. The oxygen concentration of the buffers was reduced by flushing with argon.

Superoxide radical formation was detected by EPR spectroscopy at room temperature. One mM NAD(P)H was added to 1 ml of 50 mM MES/NaOH, 50 mM NaCl, pH 6.0, containing 45 μg of complex I reconstituted in phospholipids, 100 μM decyl-ubiquinone, and 100 mM of the spin trap DEPMPO. 10 μM piericidin A was added where indicated. For control, superoxide dismutase (100 units/ml; Sigma) was added to the assay buffer. 20 μl aliquots were withdrawn from the solutions and placed in small quartz tubes in the cavity.

Amplex Red Assay—Superoxide dismutates rapidly to H_2O_2. Thus, the total rate of superoxide and H_2O_2 production was additionally measured by the horseradish peroxidase-dependent oxidation of Amplex Red (46). The 1 ml assay contained 5 μg of complex I in polar lipids, 2 units of horseradish peroxidase, and 10 μM Amplex Red. The reaction was started by the addition of 30 μM NAD(P)H. When indicated, 60 μM decyl-ubiquinone or 10 μM piericidin A was added. The oxidation of the nucleotide was followed at 340 nm; the production of resorufin was monitored at 557–620 nm (ϵ = 23.1 mM^{-1} cm^{-1}, pH 6.0) using an UV-visible diode array photometer (J&M Analytik AG, Aalen, Germany).

Other Analytical Assays—The purity of the nucleotides used in this study was determined by HPLC as described (33). Analysis was performed with a reverse phase C-18 column (5 μm Hypersil ODS, 250 × 10 mm, Knauer Wissenschaftlicher Gerätebau, Berlin, Germany) coupled with a multiwavelength detector (GE Healthcare). The mobile phase was 200 mM NaCl, 1 mM Tris/HCl, pH 8.2. NADH/ferricyanide oxidoreductase activity was measured at room temperature with an Ultrospec 1000 (GE Healthcare) spectrophotometer at 410 nm in 50 mM MES/NaOH, 50 mM NaCl, pH 6.0, using an ϵ of 1 mM^{-1} cm^{-1}. The reaction was started with 0.2 mM NADH. Protein concentrations were determined according to the biuret method.

RESULTS

Reaction of Complex I with NAD(P)H—So far, a kinetic analysis with NADPH as substrate was only reported for the mitochondrial complex I (22, 34) in submitochondrial particles. To determine the activity of a bacterial complex I with NADPH, the *E. coli* enzyme was purified by affinity chromatography from an overproducing strain (29) and reconstituted in *E. coli* polar lipids to regain full enzymatic activity (32). The kinetic parameters were calculated from the dependence of the reaction rate on the nucleotide concentration in Hanes plots (Table 1) (35). By measuring the rate of NADH oxidation at various NADH concentrations, a K_m^{NADH} of 13 μM and a V_{max} of 2.9 μmol/(min·mg) were determined. Measuring the rate of the decyl-ubiquinone reduction at various NADH concentrations led to the same K_m^{NADH} and a V_{max} of 2.8 μmol/(min·mg). The reaction was inhibited by more than 95% by an addition of 10 μM piericidin A, a specific complex I inhibitor. These data demonstrate that the physiological electron transfer from NADH to quinone was measured in the reconstituted system. The K_m^{NADPH} was determined to be 1.9 mM (Table 1). The V_{max} with NADPH as substrate was 8-fold lower than with NADH (Table 1). These data are in agreement with those reported for the mitochondrial complex (22–25).

To determine whether the oxidation of NADPH by complex I led to a reduction of the Fe/S clusters, aliquots of the preparation were treated either with NADH or NADPH and was characterized by helium temperature EPR spectroscopy. The aim was not to determine the absolute amount of the reduced clusters but to detect the difference in the degree of reduction. Therefore, the amount of the individual clusters was estimated from the amplitude of the individual signals at the g values indicated below. Redox mediators were omitted because they give a strong signal at g = 2.00 overlapping with the g_z of N1a (31). The spectra of the reconstituted complex reduced with either NADH or NADPH were very similar (Fig. 2). A comparison of both spectra revealed that NADPH reduced N1a (at g = 2.00; 40 K) by 100%, N1b (at g = 2.03, 40 K), N3 (at g = 2.04; 13 K), and N4 (at g = 2.09; 13 K) by 90% and N2 (at g = 2.05; 13 K) by 85% compared with the reduction of the Fe/S clusters by NADH, which was attributed to 100% (Fig. 2).

To investigate whether the NAD(P)H-driven redox reaction led to proton translocation, the complex was reconstituted in proteoliposomes (32), and the generation of a proton gradient was determined by the fluorescence of the pH-sensitive dye ACMA (Fig. 3). The addition of NADH gave rise to a proton gradient that was completely sensitive to the proton uncoupler CCCP and the specific inhibitor piericidin A (Fig. 3, *a* and *b*). Thus, the signal reflects the presence of a proton gradient generated by the redox reaction of the complex. No signal was obtained after an addition of 5 mM NADPH to the proteoliposomes. This could be due to the slow reaction rate of the com-

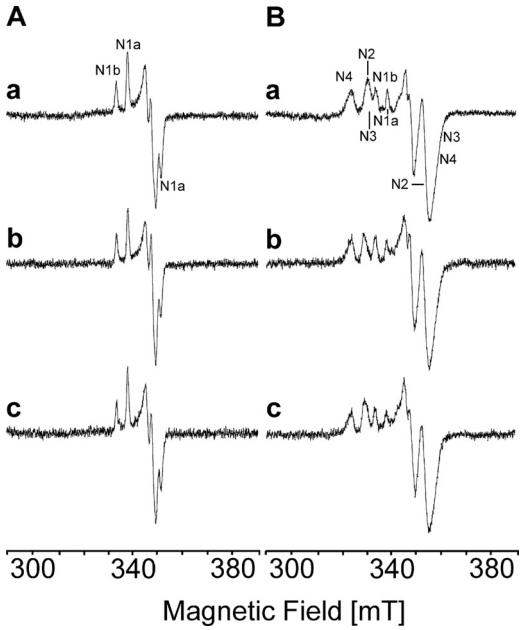

FIGURE 2. **Reduction of the Fe/S clusters of complex I and the E183H^F variant by nucleotides.** Complex I was reduced with a 1,000-fold molar excess of both NADH (*trace a*) and NADPH (*trace b*). The E183H^F variant was reduced with a 1,000-fold molar excess NADPH (*trace c*). The spectra in *A* were recorded at 40 K and 2 milliwatts of microwave power, and the spectra in *B* were recorded at 13 K and 5 milliwatts of microwave power. Other EPR conditions were as follows: microwave frequency, 9.44 GHz; modulation amplitude, 0.6 mT; time constant: 0.124 s; scan rate: 17.9 mT/min.

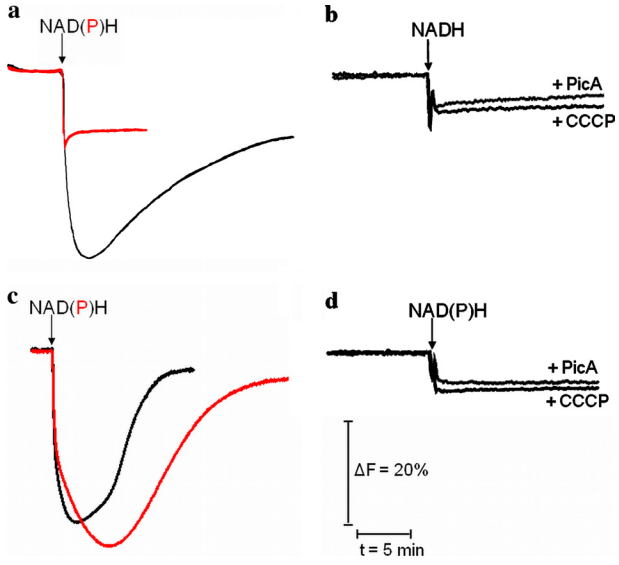

FIGURE 3. **Generation of a proton gradient by complex I and the E183H^F variant.** The proteins were reconstituted in proteoliposomes, and the ACMA fluorescence was monitored (28). The reaction of complex I (*a*) and the E183H^F variant (*c*) was started by adding either NADH (*black curve*) or NADPH (*red curve*) as indicated. The addition of NADPH to proteoliposomes containing complex I did not lead to the generation of a detectable proton gradient. As a control, either CCCP or piericidin A was added to the complex (*b*) before the reaction was started with the addition of NADH and to the variant (*d*) before the reaction was started with either NADH or NADPH.

plex with NADPH as a substrate compared with the proton leakiness of the proteoliposomes. However, it is also possible that the reaction of complex I with NADPH is not coupled with proton translocation.

Role of Glu-183^F—From the mode of NADH binding (Fig. 1), we expected Glu-183^F to be essential for the specificity of complex I for NADH. We inspected the homologues of NuoF in the databases to check whether the residue is conserved (supplemental Fig. S1). All sequences that were unambiguously identified as coding for the complex I subunit NuoF contained a glutamic acid at the homologous position.

TABLE 2
NADH/ferricyanide oxidoreductase activity (measured as ferricyanide reduction) and NAD(P)H oxidase activity (measured as oxygen consumption) of cytoplasmic membranes of various *E. coli* strains used in this study

Strain	NADH/ferricyanide oxidoreductase activity	NADH oxidase activity	NADPH oxidase activity
		$\mu mol \cdot min^{-1} \cdot mg^{-1}$	
Parental	7.0	0.8	0.2
E183D^F	15.4	1.8	1.1
E183Q^F	7.9	0.8	0.6
E183N^F	15.4	1.1	0.5
E183H^F	11.2	1.1	0.5

Structural comparisons between other NAD- and NADP-binding proteins revealed that the space needed for binding the additional phosphate group of NADP is occupied by a hydrogen bond between a conserved aspartate and the adenosine ribose as described for NAD-dependent dehydrogenases (36). To accommodate the binding of NADP, an adjustment of the nucleotide binding region is necessary (37). It has been described that either a conformational change takes place leading to a hydrogen bond between a nitrogen of the backbone and a phosphate oxygen (38) or that the aspartic acid residue is replaced by an asparagine residue forming hydrogen bonds to the adenosine ribose and the phosphate group (39). For the NADP-dependent glutathione reductase, it was shown that the high affinity of NADP binding correlates with the presence of two basic amino acid residues around NADPH's additional phosphate group (40). Because of the data reported in the literature, we replaced the conserved Glu-183^F of complex I by Asp, Gln, Asn, and His.

Generation and Characterization of Variants—The conserved Glu-183^F was mutated using an *E. coli* strain lacking all 13 genes coding for subunits of complex I on the chromosome. This strain was transformed with the 21-kb expression plasmid pBAD*nuo*$_{His}$ containing the 13 complex I genes under the control of an inducible promoter (29). Because the plasmid is too large for mutagenesis, mutations were introduced in the 6-kb plasmid pCA24N*nuoF* containing only *nuoF*. The gene *nuoF* on the plasmid pBAD*nuo*$_{His}$ was inactivated by the insertion of an *nptI-sacRB* selection cartridge via λ-Red-mediated recombination. In a second recombineering step, the inactivated gene *nuoF* was individually replaced by the mutated versions of *nuoF*, again using λ-Red-mediated recombination. All mutations were confirmed by DNA sequencing.

Cytoplasmic membranes were prepared from the mutants, and the NAD(P)H conferred activities were measured (29). Compared with the parental strain, the mutant strains E183D^F, E183N^F, and E183H^F exhibited a 2-fold increase in NADH/ferricyanide oxidoreductase activity, although that of the mutant strain E183Q^F was not significantly changed (Table 2). This indicates either an enhanced amount of complex I in the corresponding mutant membranes or an enhanced enzymatic turnover due to the mutation in the active site. The NADH

oxidase activity of the mutants E183Q^F, E183N^F, and E183H^F was only slightly enhanced, although that of the mutant E183D^F was increased more than 2-fold. In addition, the conservative substitution E183D^F led to a more than 5-fold enhanced NADPH oxidase activity, although the NADPH oxidase activity of the other mutants was increased ~2-fold (Table 2). The NAD(P)H oxidase activities were sensitive to piericidin A.

Purification and Characterization of Variants—The wild type complex and the variants were isolated from the corresponding strains by affinity chromatography (29). From 20 g of cells, ~3–4 mg of protein were obtained from all strains (supplemental Tables S3–S6), indicating that the enhanced NADH/ferricyanide oxidoreductase activity of the mutant membranes (Table 2) reflects an enhanced catalytic activity and not an increased amount of the complex I variants in the membrane. SDS-PAGE of the preparations demonstrates the presence of all complex I subunits without any significant traces of impurities (supplemental Fig. S2).

After reconstitution in lipids, the kinetic parameters of the variants for the NAD(P)H:decyl-ubiquinone oxidoreductase activity were determined (Table 1). The E183N^F and the E183Q^F variants showed a reactivity toward NADH like the complex from the parental strain. In contrast, the variants E183H^F and E183D^F exhibited a significantly higher reaction rate with NADH and higher affinity to NADH than the complex from the parental strain. All variants showed a better reactivity with NADPH than the complex from the parental strain, although to varying extents. The E183H^F variant exhibited a 3-fold higher activity with NADPH and an 75-fold higher affinity. Most strikingly, the E183D^F variant showed a 10-fold higher reaction rate with NADPH, which is even higher than the reaction rate of the complex from the parental strain with NADH. However, the affinity of the E183D^F variant to NADPH was only 5-fold greater than that of the parental strain. Although its reactivity with NADH was not significantly changed, the E183Q^F variant showed a more than 40-fold higher affinity to NADPH and a 4-fold enhanced reaction rate. The NAD(P)H:decyl-ubiquinone oxidoreductase activity of the preparations of all variants was inhibited more than 95% by piericidin A with an IC_{50} of 5 μM, which is identical to that obtained for complex I from the parental strain. Thus, the variants exhibited NADPH:ubiquinone oxidoreductase activity. The catalytic efficiency with NADH was not enhanced in the E183N^F and E183Q^F variants but was 3-fold higher in the E183D^F and E183H^F variants. Most strikingly, the catalytic efficiency with NADPH was enhanced 220-fold in the E183H^F variant, 178-fold in the E183Q^F variant, 50-fold in the E183D^F variant, and 12-fold in the E183N^F variant (Table 1).

The pH dependence of the NAD(P)H oxidase activity of bovine mitochondria has been reported in the literature (22–25). To determine the pH dependence of the *E. coli* complex I NAD(P)H:decyl-ubiquinone oxidoreductase activity, the preparation was measured in the range from pH 5 to 8 (Fig. 4). The pH activity profile of the NADH:decyl-ubiquinone oxidoreductase activity showed a broad maximum between 6.0 and 7.5 with an abrupt decrease to more acidic and more basic pH values. The NADPH:decyl-ubiquinone oxidoreductase activity showed a similar dependence with a more narrow plateau between pH 6.0 and 6.5. The contribution of the conserved Glu-183^F to the pH dependence of the activity was examined by measuring the activity of the variants at different pH values (Fig. 4). The activity profiles were very similar to that of the complex from the parental strain. The NADH oxidation profile of the E183H^F variant showed a plateau of maximum activity between pH 6.0 and 7.0 and a greater decrease to more extreme pH values. The NADPH oxidation showed a distinct activity maximum at pH 6.0 and a marked decrease to more acidic pH values but a less marked decrease to more basic pH values. As all variants showed a maximum activity at pH 6.0 to 7.0, Glu-183^F does not significantly contribute to the pH dependence of the NAD(P)H:decyl-ubiquinone oxidoreductase activity.

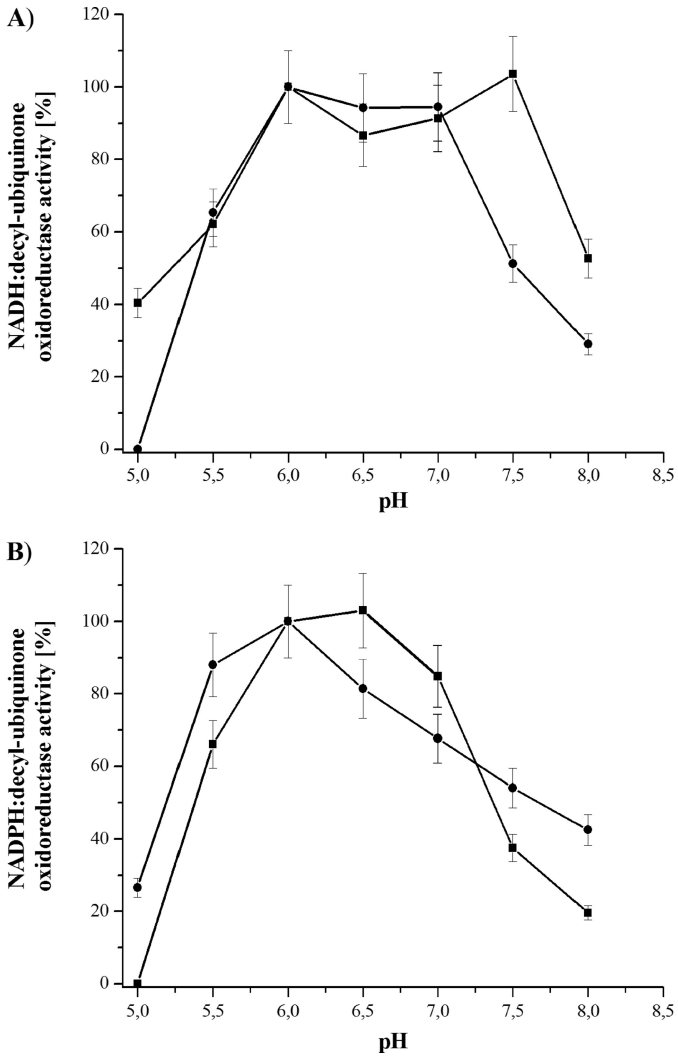

FIGURE 4. **pH dependence of the NADH:decyl-ubiquinone (*A*) and NADPH:decyl-ubiquinone (*B*) oxidoreductase activity of complex I (*squares*) and the E183H^F variant (*circles*).** The activity was measured between pH 5.0 and 8.0. All activities were more than 95% sensitive to the addition of 10 μM piericidin A. The maximum activity of the NADH and NADPH oxidation was 2.8 and 0.6 μM·min^{-1}·mg^{-1} for complex I, respectively, and 4.0 and 1.3 μM·min^{-1}·mg^{-1} for the E183H^F variant. The other variants showed a similar pH activity profile with a maximum NADH oxidation rate between pH 6.0. and 7.0 and a maximum NADPH oxidation rate between 6.0 and 6.5.

To determine whether the Fe/S clusters of the variants were reduced by NADPH, EPR spectra at helium temperature were recorded as described above. The signals of all Fe/S clusters of

the E183H^F variant were detectable after an addition of NADPH to the preparation (Fig. 2, *trace c*). A comparison with the spectra of the NADH-reduced sample of complex I from the parental strain revealed that NADPH completely reduced the EPR-detectable Fe/S clusters in this variant.

The ability of the E183H^F variant to translocate protons was examined after reconstitution in proteoliposomes (32). A pH-gradient generated by the redox reaction of complex I was detected by the ACMA fluorescence. Addition of NADH led to the generation of a pH gradient as with the wild type enzyme (Fig. 3*c*). In contrast to the wild type complex, the variant E183H^F generated a pH gradient with NADPH as a substrate. Because of the higher turnover rate with NADH compared with that of NADPH (Table 1), the rise of the gradient is faster after an addition of NADH. The ACMA signals correspond to a proton gradient established by the redox reaction of the variant as it is sensitive to piericidin A and CCCP (Fig. 3*d*). The different rate of the decay of the NADH- and NADPH-induced ACMA quench is due to the different tightness of the proteoliposomes.

Generation of Reactive Oxygen Species—Studies on mitochondria have shown that complex I-mediated lipid peroxidation due to the generation of ROS is enhanced in the presence of NADPH (41). Therefore, we examined whether an addition of either NADH or NADPH to complex I and the E183H^F variant gives rise to the formation of superoxide or hydrogen peroxide radicals. ROS were directly detected by scavenging radicals with the phosphorylated nitrone-type spin trap compound DEPMPO. The DEPMPO-OOH and DEPMPO-OH adduct radicals are easily detected by EPR spectroscopy due to their long half-life ($t_{½}$ of ~8 min) and its distinct superoxide trapping rate (42). The sample containing either complex I or the variant in phospholipids showed a similar behavior; no EPR signals were detectable in the presence of a 10-fold molar excess of decyl-ubiquinone and 100 mM DEPMPO or in the absence of any nucleotides (Fig. 5). An addition of 1 mM NADH led to a small background signal that could hardly be detected in the complex from the parental strain but was clearly present in the variant. However, the addition of 1 mM NADPH gave rise to the characteristic EPR signals of the DEPMPO-OOH adduct radical. These signals increased with time concomitant with the appearance of signals deriving from the DEPMPO-OH adduct radical. The amplitude of the signals was higher with the complex from the parental strain than with the variant. The formation of the EPR signals of the spin trap was completely suppressed by the addition of superoxide dismutase. The generation of superoxide depended on the presence of decyl-ubiquinone in the assay because the signals of the spin trap were considerably diminished in the samples lacking decyl-ubiquinone. No signals were detected after an addition of NADPH to phospholipids lacking the complex in the presence of decyl-ubiquinone. In addition, the appearance of the signals was not inhibited by an addition of piericidin A (Fig. 5).

To obtain information about the rate and the total amount of superoxide and H_2O_2 formation under various experimental conditions, the ROS production was determined by measuring the horseradish peroxidase-dependent oxidation of Amplex Red (Table 3). Neither H_2O_2 nor superoxide was produced in the absence of the nucleotides. The addition of NADH to complex I led to a limited ROS production, although the amount was enhanced more than 2-fold by the addition of NADPH. The variant showed an increased ROS production in the presence of NADH but only a slight increase after the addition of NADPH. The specific activity of complex I with NADPH is lower than that of the E183H^F variant (Table 1). However, complex I produced more ROS than the variant in the presence of NADPH (Fig. 5; Table 3). Simultaneous measurement of the NADPH oxidation rate revealed that the ROS production added up to 14% of the NADPH oxidation in complex I, whereas only 4% was used in the side reaction in the variant. Addition of piericidin A in the presence of NADPH had just a small effect on the production of superoxide and H_2O_2 by the variant but it further enhanced the production by complex I. Significantly less ROS were formed in the absence of decyl-ubiquinone in both samples. Thus, the data obtained by the Amplex Red assay are in agreement with those obtained by the spin trap method.

From these data, we propose that under these experimental conditions the ROS evolved at the NADH-binding site were mediated to a certain extent by decyl-ubiquinone, which has a

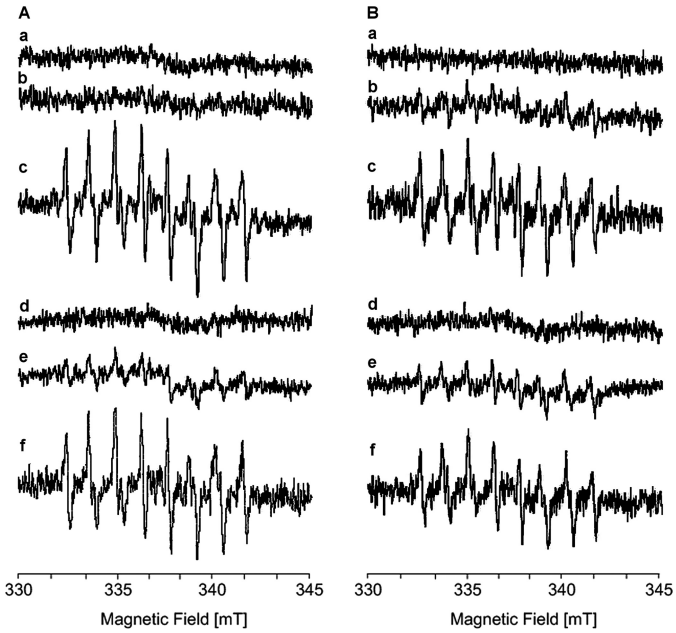

FIGURE 5. **NAD(P)H-induced superoxide production by complex I (*A*) and the E183H^F variant (*B*).** The spectra were recorded with aliquots of the proteins reconstituted with phospholipids in the presence of 100 mM DEPMPO and 100 μM decyl-ubiquinone (*trace a*), plus 1 mM NADH (*trace b*), plus 1 mM NADPH (*trace c*), plus 1 mM NADPH and superoxide dismutase (100 units/ml) (*trace d*), plus 1 mM NADPH but without decyl-ubiquinone (*trace e*), and plus 1 mM NADPH and 20 μM piericidin A (*trace f*). Other EPR conditions were as follows: microwave frequency, 9.65 GHz; modulation amplitude, 0.1 mT; time constant: 0.164 s; scan rate: 5.4 mT/min.

TABLE 3

Superoxide and H_2O_2 production by complex I and the E183H^F variant measured as Amplex Red oxidation

Piericidin A is abbreviated as PicA; decyl-ubiquinone is abbreviated as Dec-Q.

Sample	NAD(P)H-induced superoxide and H_2O_2 production				
	None	+NADH	+NADPH	+NADPH, +PicA	+NADPH, −Dec-Q
	nmol·min^{-1}·mg^{-1}				
Complex I	0	17 ± 0.3	40 ± 0.9	75 ± 1.2	26 ± 0.7
E183H^F	0	25 ± 0.4	29 ± 0.6	23 ± 0.6	11 ± 0.3

distinct water solubility. Although the E183H^F variant shows a strongly enhanced catalytic efficiency with NADPH, this reactivity is coupled with the generation of ROS. This might be due either to the low K_m^{NADPH}, which is twice the K_m^{NADH} of the complex from the parental strain, or to the slow reaction rate with NADPH, which is one-third that of the wild type complex with NADH as a substrate (Table 1). The E183D^F variant is most helpful in discriminating between these two possibilities because it exhibits a very low K_m^{NADPH} of 390 μM but has a faster reaction rate with NADPH than the wild type complex with NADH (Table 1). This variant also produces ROS under these experimental conditions (supplemental Fig. S3), demonstrating that the binding of the nucleotide determines whether ROS are produced or not.

DISCUSSION

By changing a single amino acid residue in a complex consisting of nearly 5,000 amino acid residues, we have created a novel enzymatic function, an energy-converting NADPH: ubiquinone oxidoreductase, which has so far not been described in natural systems. By replacing Glu-183^F with a histidine residue, the catalytic efficiency of the respiratory complex I with NADPH as substrate was more than 200-fold enhanced (Table 1). This is experimental proof of the assumption that Glu-183^F is a key residue in substrate recognition as derived from structural analysis. The strictly conserved Glu-183^F (supplemental Fig. S1) ensures that complex I only uses NADH *in vivo* and not NADPH. Although the catalytic efficiency of the E183H^F variant with NADH is 3-fold higher than with the wild type complex (Table 1), the mutation has not evolved in the sequenced species, most likely because the higher efficiency is at the cost of the loss of substrate selectivity. In addition, the oxidation of NADPH by the variants produced in this study is always coupled with the generation of ROS. Thus, a conserved glutamic acid residue at this position in the nucleotide binding domain of NAD-dependent dehydrogenases is indicative of a selective use of NADH (36, 37, 40, 43). Some examples in the literature discuss that it is not a trivial undertaking to change the nature of the nucleotide cofactor for dehydrogenases by site-directed mutagenesis, even in more simply structured enzymes (44).

The various mutations had different effects on the NAD(P)H oxidation kinetics (Table 1). Changing the acidic amino acids to the corresponding amides had no effect on NADH binding. The substitution to an asparagine residue increased the catalytic efficiency with NADPH 10-fold, whereas the substitution to a glutamine residue led to a 177-fold enhanced catalytic efficiency with NADPH indicating a specific interaction most likely between the amide oxygen atom of the side chain and NADPH. The data indicate that the electrostatic repulsion between the side chain carboxylate of Glu-183^F and the phosphate group bound to the adenosine ribose is the key interaction preventing a rapid oxidation of NADPH by complex I. The conservative replacement of Glu-183^F by an aspartic acid residue led to a slightly higher catalytic efficiency with NADH but to a 50-fold higher efficiency with NADPH, which can be explained by the less steric hindrance for binding NADPH. The low affinity of this variant to NADPH (Table 1) reflects the contribution of the electrostatic repulsion in this variant. The introduction of a histidine residue at this position led to a 3-fold enhanced catalytic efficiency with NADH but a drastic 220-fold increase of the efficiency with NADPH (Table 1). This might derive from a less steric hindrance at this position and an electrostatic stabilization of the negative charge of the phosphate group (40).

The single mutation neither changed the other activities of complex I such as the reduction of the Fe/S clusters (Fig. 2), the reduction of the quinone (Tables 1 and 2), and the translocation of protons (Fig. 3) nor did it influence the coupling of the processes. Using the proteoliposomes, we were not able to detect proton translocation by the complex from the parental strain with NADPH. This is most likely due to the low reaction rate of this enzyme with NADPH in combination with the proton leakiness of the proteoliposomes. The assumption that the mutations introduced resulted in NADPH-driven proton translocation is very unlikely, because the sites of nucleotide binding and proton translocation are separated by a distance of more than 100 Å (20, 21).

The oxidation of NADPH by complex I and its variants is always accompanied by ROS production, although the NADPH-induced ROS production is slightly diminished in the variants (Fig. 5; Table 3). However, they also show, in contrast to the wild type complex, an NADH-induced ROS production. The source of ROS evolving during the redox reaction of complex I is still under discussion (45). Most investigators agree on the flavin site, whereas the ubiquinone-binding site and the Fe/S clusters N1a and N2 have also been proposed to be responsible for the generation of ROS (46). Recently, it was proposed that the site where ROS are generated is variable and determined by the reduction state of the individual cofactors (47). Thus, the various sites of ROS production reported under different experimental conditions might derive from different states of the complex (47). Under our experimental conditions the ROS are produced at the flavin site because piericidin A did not inhibit ROS production (Fig. 5 and Table 3).

The E183D^F variant, exhibiting a higher maximal reaction rate with NADPH than complex I with NADH and a very low affinity to NADPH (Table 1), showed an NADPH-induced ROS production. In addition, the NADPH-induced ROS production is enhanced in complex I compared with the E183H^F variant (Fig. 3; Table 3) because the portion of electrons involved in the side reaction leading to ROS production is more than 4-fold enhanced. These data indicate that the mode of nucleotide binding contributes to the possibility of ROS being generated at this site. To understand the molecular details of this process, a high resolution structure of the nucleotide-binding site of complex I with bound NADP(H) is needed.

Acknowledgments—We kindly thank Helga Lay for an excellent HPLC analysis of the nucleotides and Lothar Kussmaul and Karoline Aierstock, Boehringer Ingelheim, for their help in establishing the Amplex Red assay. We are grateful to Linda Williams for help in preparing the manuscript.

REFERENCES

1. Weiss, H., Friedrich, T., Hofhaus, G., and Preis, D. (1991) *Eur. J. Biochem.* **197,** 563–576
2. Walker, J. E. (1992) *Q. Rev. Biophys.* **25,** 253–324
3. Ohnishi, T. (1998) *Biochim. Biophys. Acta* **1364,** 186–206
4. Friedrich, T. (2001) *J. Bioenerg. Biomembr.* **33,** 169–177
5. Yagi, T., and Matsuno-Yagi, A. (2003) *Biochemistry* **42,** 2266–2274
6. Brandt, U. (2006) *Annu. Rev. Biochem.* **75,** 69–92
7. Carroll, J., Fearnley, I. M., Skehel, J. M., Shannon, R. J., Hirst, J., and Walker, J. E. (2006) *J. Biol. Chem.* **281,** 32724–32727
8. Friedrich, T. (1998) *Biochim. Biophys. Acta* **1364,** 134–146
9. Friedrich, T., and Scheide, D. (2000) *FEBS Lett.* **479,** 1–5
10. Friedrich, T., and Böttcher, B. (2004) *Biochim. Biophys. Acta* **1608,** 1–9
11. Baranova, E. A., Holt, P. J., and Sazanov, L. A. (2007) *J. Mol. Biol.* **366,** 140–154
12. Sazanov, L. A., and Hinchliffe, P. (2006) *Science* **311,** 1430–1436
13. Berrisford, J. M., and Sazanov, L. A. (2009) *J. Biol. Chem.* **284,** 29773–29783
14. Dupuis, A., Prieur, I., and Lunardi, J. (2001) *J. Bioenerg. Biomembr.* **33,** 159–168
15. Fendel, U., Tocilescu, M. A., Kerscher, S., and Brandt, U. (2008) *Biochim. Biophys. Acta* **1777,** 660–665
16. Friedrich, T., and Weiss, H. (1997) *J. Theor. Biol.* **187,** 529–540
17. Mathiesen, C., and Hägerhäll, C. (2003) *FEBS Lett.* **549,** 7–13
18. Brandt, U., Kerscher, S., Dröse, S., Zwicker, K., and Zickermann, V. (2003) *FEBS Lett.* **545,** 9–17
19. Mamedova, A. A., Holt, P. J., Carroll, J., and Sazanov, L. A. (2004) *J. Biol. Chem.* **279,** 23830–23836
20. Efremov, R. G., Baradaran, R., and Sazanov, L. A. (2010) *Nature* **465,** 441–445
21. Hunte, C., Zickermann, V., and Brandt, U. (2010) *Science* **329,** 448–451
22. Vinogradov, A. D. (1998) *Biochim. Biophys. Acta* **1364,** 169–185
23. Hatefi, Y., and Hanstein, W. G. (1973) *Biochemistry* **12,** 3515–3522
24. Djavadi-Ohaniance, L., and Hatefi, H. (1975) *J. Biol. Chem.* **250,** 9397–9403
25. Rydström, J., Montelius, J., Bäckström, D., and Ernster, L. (1978) *Biochim. Biophys. Acta* **501,** 370–380
26. Datsenko, K. A., and Wanner, B. L. (2000) *Proc. Natl. Acad. Sci. U.S.A.* **97,** 6640–6645
27. Court, D. L., Sawitzke, J. A., and Thomason, L. C. (2002) *Annu. Rev. Genet.* **36,** 361–388
28. Pohl, T., Bauer, T., Dörner, K., Stolpe, S., Sell, P., Zocher, G., and Friedrich, T. (2007) *Biochemistry* **46,** 6588–6596
29. Pohl, T., Uhlmann, M., Kaufenstein, M., and Friedrich, T. (2007) *Biochemistry* **46,** 10694–10702
30. Kitagawa, M., Ara, T., Arifuzzaman, M., Ioka-Nakamichi, T., Inamoto, E., Toyonaga, H., and Mori, H. (2005) *DNA Res.* **12,** 291–299
31. Leif, H., Sled, V. D., Ohnishi, T., Weiss, H., and Friedrich, T. (1995) *Eur. J. Biochem.* **230,** 538–548
32. Stolpe, S., and Friedrich, T. (2004) *J. Biol. Chem.* **279,** 18377–18383
33. Markham, K. A., Sikorski, R. S., and Kohen, A. (2004) *Anal. Biochem.* **325,** 62–67
34. Albracht, S. P., Mariette, A., and de Jong, P. (1997) *Biochim. Biophys. Acta* **1318,** 92–106
35. Hanes, C. S. (1932) *Biochem. J.* **26,** 1406–1421
36. Lesk, A. M. (1995) *Curr. Opin. Struct. Biol.* **5,** 775–783
37. Mittl, P. R., Berry, A., Scrutton, N. S., Perham, R. N., and Schulz, G. E. (1994) *Protein Sci.* **3,** 1504–1514
38. Thorn, J. M., Barton, J. D., Dixon, N. E., Ollis, D. L., and Edwards, K. J. (1995) *J. Mol. Biol.* **249,** 785–799
39. Phillips, C., Gover, S., and Adams, M. J. (1995) *Acta Crystallogr. D Biol. Crystallogr.* **51,** 290–304
40. Scrutton, N. S., Berry, A., and Perham, R. N. (1990) *Nature* **343,** 38–43
41. Glinn, M. A., Lee, C. P., and Ernster, L. (1997) *Biochim. Biophys. Acta* **1318,** 246–254
42. Vasquez-Vivar, J., Kalyanaraman, B., and Kennedy, M. C. (2000) *J. Biol. Chem.* **275,** 14064–14069
43. Schulz, G. E. (1992) *Curr. Opin. Struct. Biol.* **2,** 61–67
44. Dudek, H. M., Torres Pazmiño, D. E., Rodríguez, C., de Gonzalo, G., Gotor, V., and Fraaije, M. W. (2010) *Appl. Microbiol. Biotechnol.* **88,** 1135–1143
45. Hirst, J., King, M. S., and Pryde, K. R. (2008) *Biochem. Soc. Trans.* **36,** 976–980
46. Kussmaul, L., and Hirst, J. (2006) *Proc. Natl. Acad. Sci. U.S.A.* **103,** 7607–7612
47. Ohnishi, S. T., Shinzawa-Itoh, K., Ohta, K., Yoshikawa, S., and Ohnishi, T. (2010) *Biochim. Biophys. Acta* **1797,** 1901–1909
48. Bondi, A. (1964) *J. Phys. Chem.* **68,** 441–451
49. Pettersen, E. F., Goddard, T. D., Huang, C. C., Couch, G. S., Greenblatt, D. M., Meng, E. C., and Ferrin, T. E. (2004) *J. Comput. Chem.* **25,** 1605–1612